Hindawi
Shock and Vibration
Volume 2022, Article ID 5241257, 13 pages
https://doi.org/10.1155/2022/5241257

Research Article

Ground Motion and Site Characteristics Evaluation Using Hilbert-Huang Transform Method Based on Light-Moderate Earthquakes

Jinchang Chen,[1] Lanmin Wang ,[2,3] Ailan Che ,[4] and Hanxu Zhou[5]

[1]*School of Naval Architecture, Ocean and Civil Engineering, Shanghai Jiao Tong University, Shanghai 200040, China*
[2]*Lanzhou Institute of Seismology, China Earthquake Administration, Lanzhou 730000, China*
[3]*Key Lab of Loess Earthquake Engineering, China Earthquake Administration, Lanzhou 730000, China*
[4]*School of Naval Architecture, Ocean and Civil Engineering, Shanghai Jiao Tong University, Shanghai 200040, China*
[5]*School of Naval Architecture, Ocean and Civil Engineering, Shanghai Jiao Tong University, Shanghai 200040, China*

Correspondence should be addressed to Lanmin Wang; wanglm2304@126.com

Received 14 April 2022; Accepted 15 July 2022; Published 12 August 2022

Academic Editor: Pengfei Wang

Compared with strong earthquakes (Ms ≥ 6.0), light-moderate earthquakes (Ms 4–5.9) occurred more frequently and distributed more widely, and rich ground motions have been collected around world. It provides a solid data base for the investigation on the ground motion and regional site characteristics which are closely related to seismic geological disaster. We chose two light-moderate earthquakes in China as study cases. Based on Hilbert-Huang transform, we analyzed the ground motion characteristics in time-frequency domain. Using a stable coda wave and marginal spectrum of it based on horizontal to vertical Fourier spectral ratio (HVSR) method, the site characteristics are clarified. Result shows that the amplitude (instantaneous frequency energy) of Hilbert-Huang spectrum is mainly concentrated within 20 Hz at the stations that are close to epicenter. The energy will change from concentration to divergence in time and frequency and decrease with the increase of epicenter distance under soil site condition. Two earthquakes present a low prominent frequency characteristic (1.075–2.45 Hz). Hilbert energy at soil layer is about 3 times greater than it at rock site when the epicenter distance is close and soil layer can also amplify the instantaneous energy. The predominant frequency of site at each station is within 3.6–6.2 Hz. The predominant frequencies of the earthquakes are lower than the predominant frequencies of the sites and would not produce resonance effects. The result can provide meaningful references for later study works about the characteristics and application of light-moderate earthquakes.

1. Introduction

Ground motion and regional site characteristics are closely related to seismic geological disaster. The seismic response of slope will be significantly amplified, when the predominant frequency of ground motion approaches the natural frequency of slope [1]. The comparative study on the ground motion of bedrock site and soil site with close epicenter distance shows that the ground motion of bedrock site is much smaller than that of soil site, which is mainly due to the amplification effect of soil site on ground motion [2, 3]. Previous studies focused on the characteristics and effects of strong earthquakes (Ms ≥ 6.0), because large casualties and natural disasters were caused [4–6]. However, there are fewer large earthquakes with rich near-field waveform records on the mainland. Therefore, it is difficult to clarify the general law and site characteristics from these earthquakes. Correspondingly, there are many light-moderate earthquakes (Ms 4–5.9) with wide geographical distribution. With the development of observation technology, many light-moderate earthquakes have been recorded, and rich ground motion data have been accumulated all over the world. Using light-moderate earthquakes can comprehensively clarify the regional site characteristics and reveal the correlation between ground motion characteristics and disasters in a wider range. Meanwhile, light-moderate earthquakes also induced many disasters in history. For example, in 1995, an earthquake with magnitude of Ms 5.8 occurred at Yongdeng, Gansu province, China. Ten people died in the earthquake, which was mainly caused by the loess landslides [7]. A Ms 5.2 earthquake with shallow source depth occurred in Minxian-Zhangxian, Gansu province, China on November 13, 2003. In the earthquake, one person died and 26 people were injured, 3344 houses collapsed, and 3052 buildings became dangerous [8]. Relative studies to light-moderate earthquakes have been performed. A series of moderate earthquakes (M 5.8–6.5) in western Gulf greatly impacted the marine sedimentary [9]. The dynamical process of ionosphere following a moderate magnitude earthquake ($M \approx 5.9$) has been studied [10]. Ground motion prediction equation was proposed to assess the probabilistic seismic hazard in low-to-moderate seismic areas [11]. The characteristics of soil radon (Rn-222) during a series of moderate earthquakes (M 4.5–5.8) were clarified [12]. In low-to-moderate earthquake areas, non-uniform Timoshenko beam models have been used to assess the seismic performance of buildings [13]. As for the investigation about ground motion and regional site characteristics, and the relationship with seismic geological disasters using light-moderate earthquakes is insufficient.

Seismic ground motion analysis enables us to know the natural characteristics of earthquakes and the stratum conditions. It is the base for further geotechnical disaster prevention, seismic design of structures, and seismological research. Time domain analysis of signals can reflect the characteristics of amplitude with time and the attenuation law and attenuation model of amplitude. However, frequency information of signal cannot be clarified. Fourier transform is widely used in seismic signal or ambient vibration [14, 15]; however, it is only suitable for linear and stationary data analysis in theory. The seismic wave triggered by an earthquake is a kind of sudden event, which can be regarded as a nonlinear and nonstationary process, which makes it difficult to apply the seismic signal processing technology based on the traditional linear stationary system theory. Hilbert-Huang transform (HHT) can be used for nonlinear and nonstationary data analysis, which developed rapidly in recent years and is used in many fields [16–20]. Especially in mining engineering, the structure and rock mass under different stress state show different spectral characteristics during failure process [21–25].

For the record of microtremors, HVSR methods were often used to evaluate the site effects. The method is based on two assumptions [26]: 1. The vertical and horizontal values (amplitude and spectrum components) on the bedrock are equivalent; 2. The soil layer has a significant impact on the horizontal vibration, while it has little impact on the vertical vibration in the frequency components. It represents the transfer function of the surface horizontal component to the bedrock horizontal component, and the reference site is no longer needed. Studies [27] verified that the HVSR of light-moderate earthquake records can identify the amplification effect of the site, at least its resonance frequency domain. Later, this method was extended to analyze seismic response of nonlinear sites. Lermo & Chavez Garcia (1993) [28] analyzed the transfer functions of three sites in different cities in Mexico. The results of HVSR are very close to the transfer function obtained directly from the records. It shows that the predominant period and local amplification level of simple geological conditions can be obtained by the method. Bonilla, F. et al. [27] used direct S-wave, coda, and HVSR to estimate the site amplification effect in San Fernando Valley, California. The results show that the dominant period of site effect estimated by HVSR is the same as that calculated by direct S-wave and coda method, but the amplification effect is smaller. For microtremors or near-field vibration of light-moderate earthquakes, hypothesis 1 may be acceptable, but it is impossible for large earthquakes, especially for far-field nonlinear response in large earthquakes [29]. It reflects that site characteristics can be evaluated based on light-moderate earthquakes using HVSR method.

We chose two light-moderate earthquakes with magnitude Ms 5.0 and Ms 4.9 that occurred in loess area of China as study cases and investigated the spectrum characteristics of them based on HHT method in the study. First, all the seismic waves recorded by different strong motion stations that in different site conditions and epicenter distances were performed baseline correction. Second, the seismic waves were decomposed into a series of Intrinsic Mode Functions (IMFs) through Empirical mode decomposition (EMD) and each of them satisfied the hypothesis of Hilbert transform. Third, the correlation coefficients between IMFs and original signal were calculated, and the seismic signals were reconstructed by eliminating the IMFs that have low correlation with the original signal. Forth, Hilbert transform was performed on the reconstructed signal. Then, the Hilbert-Huang spectrum, marginal spectrum, and instantaneous energy spectrum of each seismic wave were obtained. We analyzed the three types of spectrums of light-moderate earthquakes and clarified the characteristics of them from time-frequency domain. At last, the site characteristics are discussed based on the coda wave of the light-moderate earthquakes using HVSR method.

2. Case Study

Light-moderate earthquakes (Ms 4–5.9) frequently occurred in Gansu Province, China. More than 119 light-moderate earthquakes occur in loess area of China from June 1, 1980 to October 28, 2019, which include 96 earthquakes with magnitude Ms 4–4.9 and 23 earthquakes with magnitude Ms 5–5.9. This study chose two typical light-moderate earthquake events in the area as study cases.

The locations of epicenter of two earthquakes and the strong motion stations were shown in Figure 1. The elevation of the area changed from 1224 m to 5218 m. Many faults distributed in this area such as Yumushan, Minle-Damaying, Huangcheng-Shuangta, Lenglongling, and Longshoushan. So, earthquakes frequently occur in this area. A Ms 5.0 earthquake with source depth about 11 km occurred on September 16, 2019. In the study area, two strong motion stations which are HZH and MLE recorded this event, as it is shown in Figure 1. Another Ms 4.9 earthquake with source depth about 16 km also occurred on May 11, 2012. In the

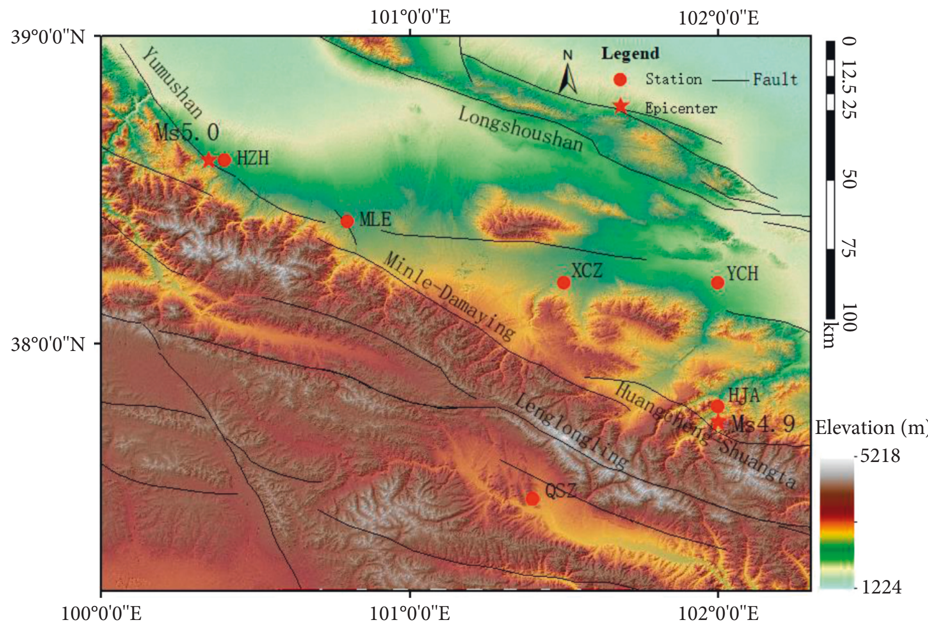

Figure 1: Study area and location of epicentral and strong motion stations.

area, four strong motion stations recorded the event, which are HJA, XCZ, YCH, and QSZ. The location, elevation, and epicenter distance of each strong motion station was shown in Table 1. It shows that HZH and HJA stations are about 2.4 km and 5.7 km away from the epicenter of Ms 5.0 and Ms 4.9, respectively, which can reflect many meaningful natural information of the two earthquake events. Among these stations, QSZ is on the rock site and with epicenter distance close to YCH and XCZ which are on soil sites. So, it can reflect the effect of site conditions on the ground motions.

3. Method

HHT is composed of two parts which are EMD and Hilbert Transform [17]. First, the signal is processed by EMD to obtain a series of IMFs, and each order of IMF can satisfy the hypothesis of Hilbert transform; Second, each order of IMF is to perform Hilbert transform to obtain Hilbert-Huang spectrum, Hilbert marginal spectrum, and instantaneous energy spectrum.

According to the theory of EMD, every time history of signal X(t) can be decomposed into n IMFs with frequency from high to low and a $r(t)$, as it is shown in:

$$x(t) = \sum_{i=1}^{n} IMF_i(t) + r(t), \quad (1)$$

where IMF_1, IMF_2, IMF_3 ... are the Intrinsic Mode Functions of different frequencies from high to low; $r\ (t)$ is residual.

Based on EMD, the intrinsic mode functions of seismic waves recorded by HZH-EW were obtained, as shown in Figure 2. The duration of original signal is 76.87 s. Peak value 71.573 cm/s^2 occurred at 23.56 s. The seismic wave was decomposed into 10 IMF with frequency from high to low and a residual. From IMF1 to IMF10, the amplitude gradually decreases, and IMF1-5 contain the most of amplitude of the original seismic wave.

In the IMFs, some low frequency components are generated by numerical error and do not have any effects on the original signal. In order to acquire the useful components, the threshold of each signal was established [30]. The calculation method of threshold value ρ for extracting useful signals was shown in (2). When $\mu_i \geq \rho$, the former IMF_i were retained, and the remaining IMF were eliminated [17].

$$\rho = \frac{\max(\mu_i)}{10\max(\mu_i) - 3}, \quad i = 1, 2 \ldots n, \quad (2)$$

where μ_i represents the correlation coefficient of the IMF_i to the original signal; n is total number of IMFs.

The correlation coefficients were shown in Figure 3. The threshold of intrinsic mode functions of seismic waves recorded by HZH-EW is 0.16 according to the calculation method mentioned in (2). The correlation coefficients of IMF1-5 greater than threshold, which were retained. The correlation coefficients of IMF6-10 close to 0, which were eliminated. The IMF2 has the most correlation with original signal and the correlation coefficient up to 0.8. Then, the reconstructed signal composed by IMF1-5 was used to make Hilbert transfer.

After the original signals were decomposed by EMD and extracted the useful components, the instantaneous frequency corresponding to each of IMF_i is calculated by Hilbert transform. Hibert-Huang spectrum is obtained. As it is shown in:

$$H(t, w) = \sum_{i=1}^{n} a_i(t, w_i), \quad (3)$$

where $\omega_i\ (t)$ is the instantaneous frequency corresponding to each of IMF_i; $a_i\ (t, w_i)$ is the amplitude corresponding to ω_i (t) of the IMF_i at certain a time t; $H\ (t,\ \omega)$ is time-frequency distribution of the amplitude of the whole signal.

Table 1: Details about each strong motion station.

Magnitude	Epicenter	Strong motion stations	Location	Epicentral distance (km)	Elevation (m)	Site condition
Ms 5.0	100.35 E, 38.6 N	HZH	100.4 E, 38.6 N	2.4	2186	Soil
		MLE	100.8 E, 38.4 N	38.42	2383	Soil
Ms 4.9	102 E, 37.75 N	HJA	102 E, 37.8 N	5.7	2774	Soil
		YCH	102 E, 38.2 N	50.25	2011	Soil
		QSZ	101.4 E, 37.5 N	59.81	3085	Rock
		XCZ	101.5 E, 38.2 N	66.5	2511	Soil

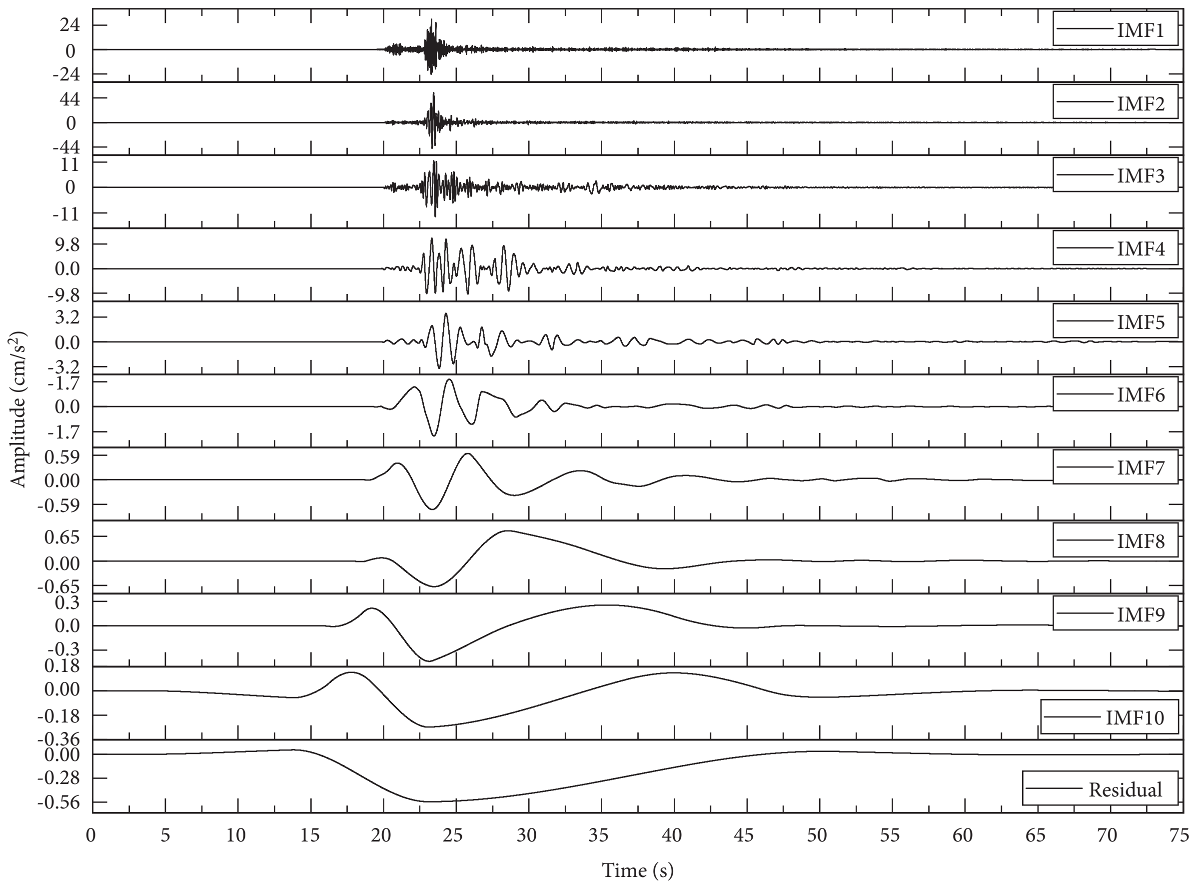

Figure 2: Intrinsic mode functions (IMFs) of HZH-EW.

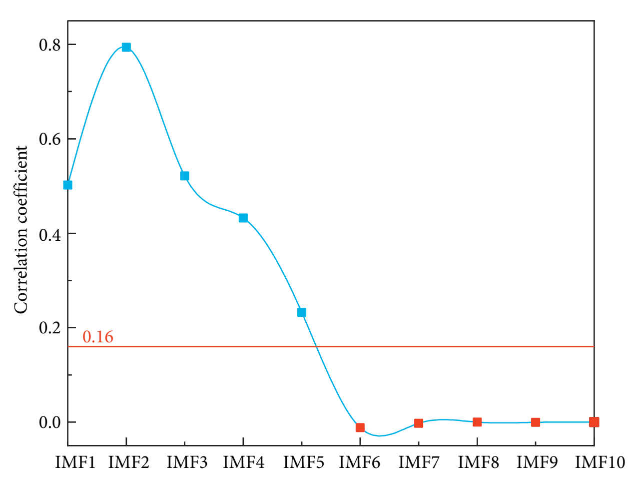

Figure 3: Correlation coefficient distribution.

The Hilbert marginal spectrum is shown in:

$$h(w) = \int_0^T H(t, w)\mathrm{d}t. \tag{4}$$

The instantaneous energy spectrum is acquired by integrating the $H^2(t, w)$ in frequency. As it shows in:

$$IE(t) = \int_w H^2(t, w)\mathrm{d}w. \tag{5}$$

All the seismic waves were performed baseline correction at first in this study. The calculation process of the HHT is implemented based on MATLAB software.

4. Results

4.1. Spectrum Characteristics of Strong Motion

4.1.1. Hilbert-Huang Spectrum Characteristics. Hilbert-Huang spectrums of seismic waves recorded by station HZH, MLE, HJA, XCZ, YCH, and QSZ were shown in Figures 4 and 5 respectively. Every station records the seismic wave with three directions and we just list the results of EW and NS directions for the amplitude of UD direction is much smaller than EW and NS directions. In the Hilbert-Huang spectrum, the relationship among time, frequency, and energy can be obtained. The amplitude of the spectrum represents the energy of instantaneous frequency.

The Hilbert-Huang spectrums of seismic waves of Ms 5.0 recorded by two strong motion stations were shown in Figure 4. Results show that the Hilbert-Huang spectrums of two stations with different epicenter distances show totally different characteristics and the distribution has certain similarity at the same station in different directions. The spectrum of HZH-EW shows that the energy concentrated at 20–30 s and instantaneous frequency concentrated within 20 Hz. Compared with HZH-EW, the energy of HZH-NS also concentrated at 20–30 s and instantaneous concentrated within 20 Hz, but peak value gradually shifts to relative high frequency (close to 20 Hz). The spectrum of MLE-EW shows that the energy widely distributed at 15–40 s and instantaneous frequency distributed within 40 Hz. Similarly, the energy of seismic wave which recorded by MLE-NS also distributed within 40 Hz. Except for the distribution characteristics, the amplitudes of two stations also have quite a difference. The peak energy of HZH-EW is about 62.3 $\mathrm{cm/s^2}$ and HZH-NS is about 41.2 $\mathrm{cm/s^2}$; however, the energy of MLE-EW is 4.6 $\mathrm{cm/s^2}$, and MLE-NS is 4.0 $\mathrm{cm/s^2}$. The peak amplitude of HZH-NS is about 10 times greater than MLE-NS and the HZH-EW is more than 10 times greater than MLE-EW, which reflect that the energy of seismic wave will changes from concentration to divergence in time and frequency and gradually decreases with the increase of epicenter distance.

The Hilbert-Huang spectrums of Ms 4.9 were shown in Figure 5. The spectrums of HJA-EW and HJA-NS show that the energy concentrated at 20–25 s and instantaneous frequency concentrated within 20 Hz. The peak amplitude of HJA-EW is about 30 $\mathrm{cm/s^2}$ and the peak value of HJA-NS is about 25 $\mathrm{cm/s^2}$. The location of YCH has the same longitude as HJA and lower elevation than HJA. The energy of seismic wave at YCH station is distributed within 10–40 s and with instantaneous frequency within 30 Hz. The peak values are 4.5 $\mathrm{cm/s^2}$ and 5.2 $\mathrm{cm/s^2}$ in the directions of EW and NS, respectively. Compared with the HJA, energy at YCH is more scattered and the peak value decreases about 5 times, which reflects that seismic energy attenuates with the epicenter distance increasing. The distribution of energy at station XCZ is more scattered compared with other stations and the peak amplitudes are 3.12 $\mathrm{cm/s^2}$ and 2.60 $\mathrm{cm/s^2}$, respectively, which are smaller than YCH, because the epicenter distance of XCZ is more far than YCH. The energy of seismic wave recorded by QSZ is concentrated at 20–25 s, the instantaneous frequency is concentrated within 20 Hz, and the peak amplitude are 1.5 $\mathrm{cm/s^2}$ and 1.58 $\mathrm{cm/s^2}$ in the directions of EW and NS, respectively. The epicenter distance of QSZ is between YCH and XCZ, whereas the energy of it is very concentrated compared with YCH and XCZ and the energy is smallest among them. This is because the site condition of QSZ station is rock, which is different from others. The results reflect that site conditions can significantly influence the distribution characteristics of instantaneous frequency energy. The energy of a seismic wave is more divergent in the soil than it is in the rock in the process of seismic wave propagation, the distribution characteristics of instantaneous frequency energy are closer to epicenter compared to the soil site condition, and the soil layer can greatly amplify the instantaneous frequency energy.

4.1.2. Marginal Spectrum Characteristics. Marginal spectrum reflects the distribution law of Hilbert energy with frequency. Hilbert energy Marginal spectrum is different from Fourier spectrum. Marginal spectrum is based on the HHT and its frequency is a function of time. So, the frequency in marginal spectrum may not necessarily appear in the whole period, but at a certain time or several times [31].

The marginal spectrums of Ms 5.0 and Ms 4.9 seismic waves at different strong motion stations were shown in Figures 6(a) and 6(b), respectively. Result shows that the shapes of marginal spectrum in N-S and E-W directions are similar with each other at each station and Hilbert energy of frequency mainly distributed within 20 Hz. Peak Hilbert energy of HZH-NS is about 23.9 and the energy is about 4.0 at MLE-NS, which reflects that peak amplitude of HZH-NS is about 6.6 times greater than MLE-NS. Peak amplitudes of HZH-NS and MLE-NS occurred at 1.125 Hz. Peak amplitudes of HZH-EW and MLE-EW occurred at 1.625 Hz and 1.375 Hz, respectively, and peak amplitude of HZH-EW is about 6.03 times greater than MLE-EW. Hilbert energy of Ms 5.0 seismic waves shows a downward trend with the increase of epicenter distance and presents low prominent frequency characteristics. The energy of HJA, XCZ, YCH, and QSZ also mainly distributed within 20 Hz and the predominant frequency was within 1.075–2.45 Hz which shows low prominent frequency characteristic. The peak Hilbert energy of HJA, YCH, QSZ, and XCZ are 5.8, 4.7, 0.59, and 0.65, respectively, which shows a decreasing trend with the increase of epicenter distance except for QSZ. Result

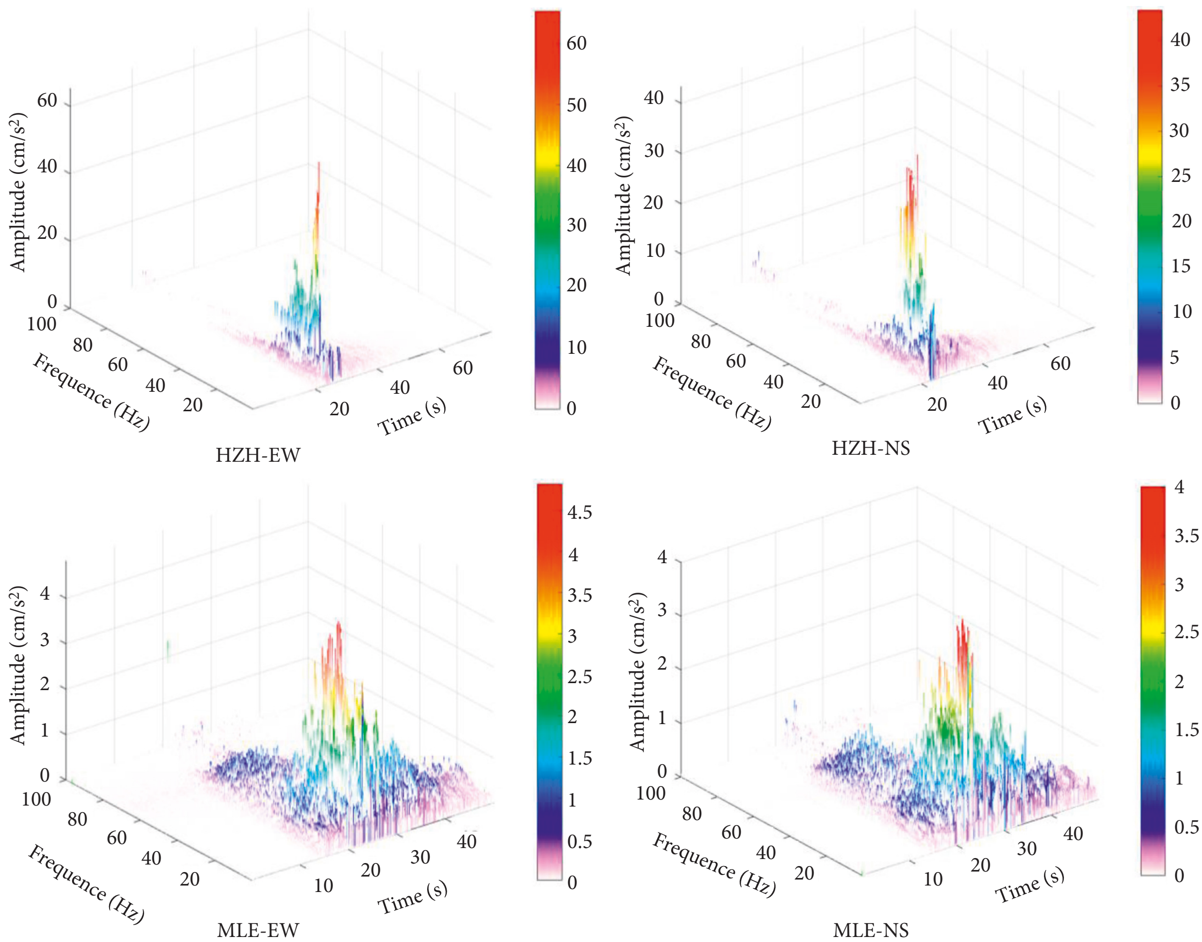

Figure 4: Hilbert-Huang spectrum of the reconstructed signal of HZH and MLE.

shows that the epicenter distance of XCZ is larger than QSZ, whereas the peak value is greater than QSZ. This result is related to the site conditions of two stations, which reflects that soil layer can greatly amplify the Hilbert energy of an earthquake. The result is consistent with the result of Hilbert-Huang spectrum.

Above results show that the prominent frequencies of the seismic waves of two earthquakes present low frequency (1.125–1.625 Hz and 1.075–2.45 Hz, respectively), the Hilbert energy shows a decreasing trend with the increase of epicenter distance, and the loess layer can amplify the Hilbert energy.

4.1.3. Instantaneous Energy Spectrum Characteristics. Instantaneous energy is an energy corresponding to time, which can reflect the instantaneous energy fluctuation of earthquakes in the whole duration.

Instantaneous energy spectrums of different strong motion stations were shown in Figure 7. Result shows that the instantaneous energy at HZH is concentrated within 20–30 s and the amplitude of two directions up to maximum value at the same time. The instantaneous energy of MLE distributed within 15–40 s and the time that amplitude of MLE-EW up to maximum is before MLE-NS. The peak amplitudes of HZH and MLE in EW direction are 7.45×10^5 and 6.45×10^3, respectively, which are about 1.6–1.7 times greater than it in NS direction. The peak value of instantaneous energy of HZH is larger than that of MLE, which reflects that the instantaneous energy attenuates quickly with the increase of epicenter distance. The instantaneous energy of HJA concentrated within 20–25 s and the amplitude in two directions up to peak is also at the same time. The peak value of HJA-EW is 2.4×10^5, which is about 1.67 times larger than HJA-NS which is about 1.6×10^5. The instantaneous energy of XCZ is distributed within 10–40 s and the time that amplitude of two directions up to maximum is same. The peak value of XCZ-EW is about 1.36 times greater than XCZ-NS. The instantaneous energy of YCH is distributed within 20–50 s and the time that peak amplitude of YCH-EW and YCH-NS occurred is different. The results show that the peak amplitude of NS direction is larger than EW at YCH. The instantaneous energy of QSZ is concentrated within 20–30 s and the time that peak amplitude of QSZ-EW and QSZ-NS occurred is different. The peak value of QSZ-NS is about 2.3 times larger than QSZ-EW. The results reflect that distribution characteristics of instantaneous energy spectrum in two directions are not unified. The peak value of EW is larger than NS at HJA and XCZ, but the value has the opposite characteristics at YCH and QSZ. The

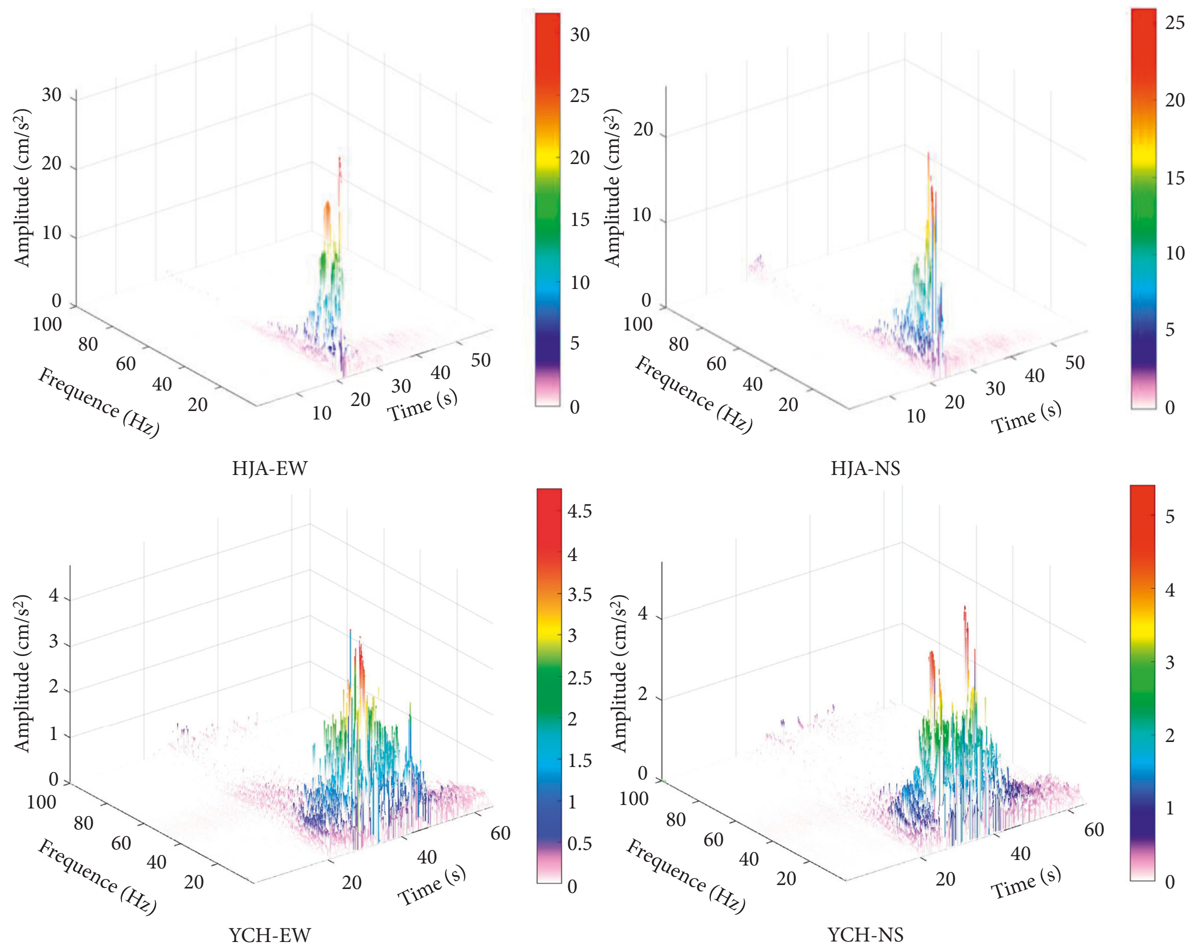

Figure 5: Continued.

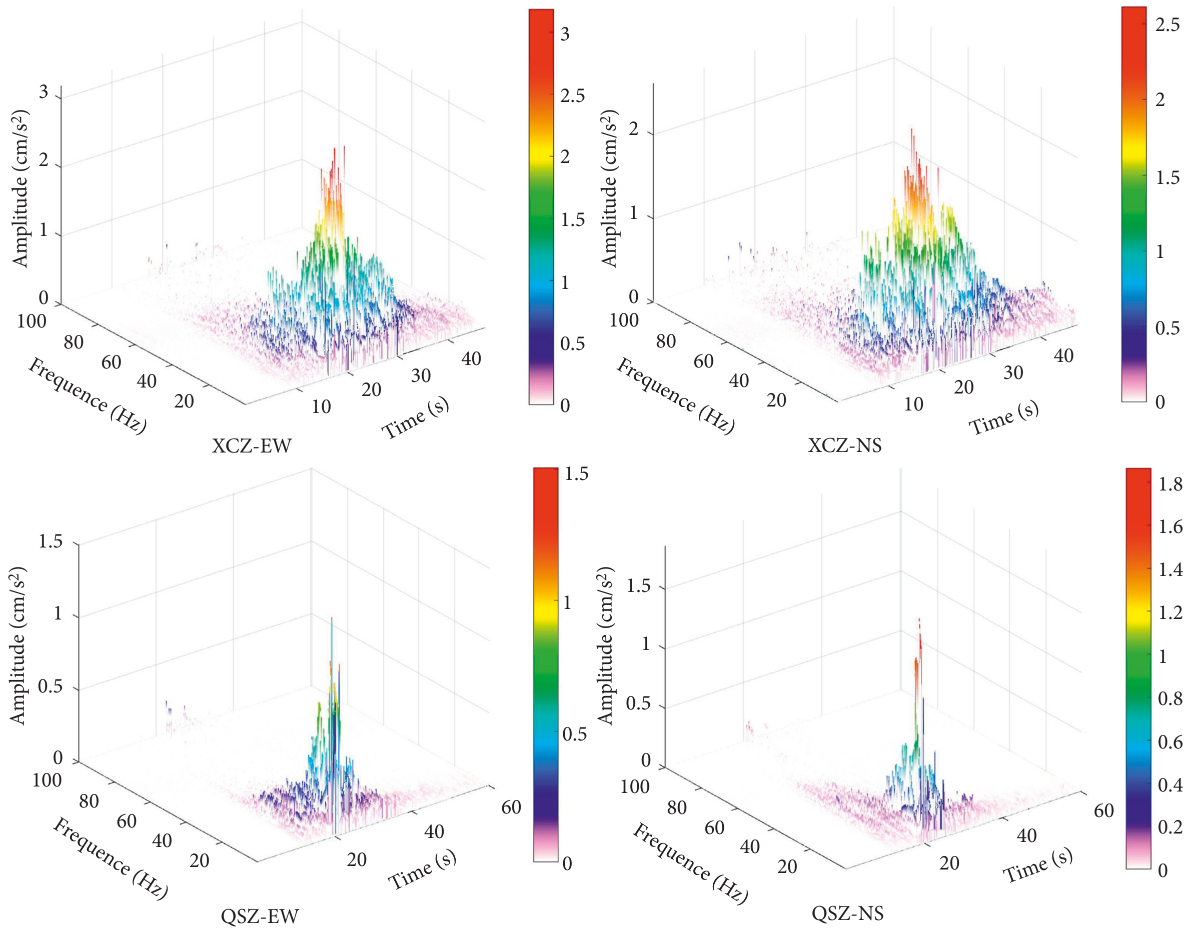

(b)

Figure 5: Hilbert-Huang spectrum of the reconstructed signal of HJA, YCH, XCZ, and QSZ.

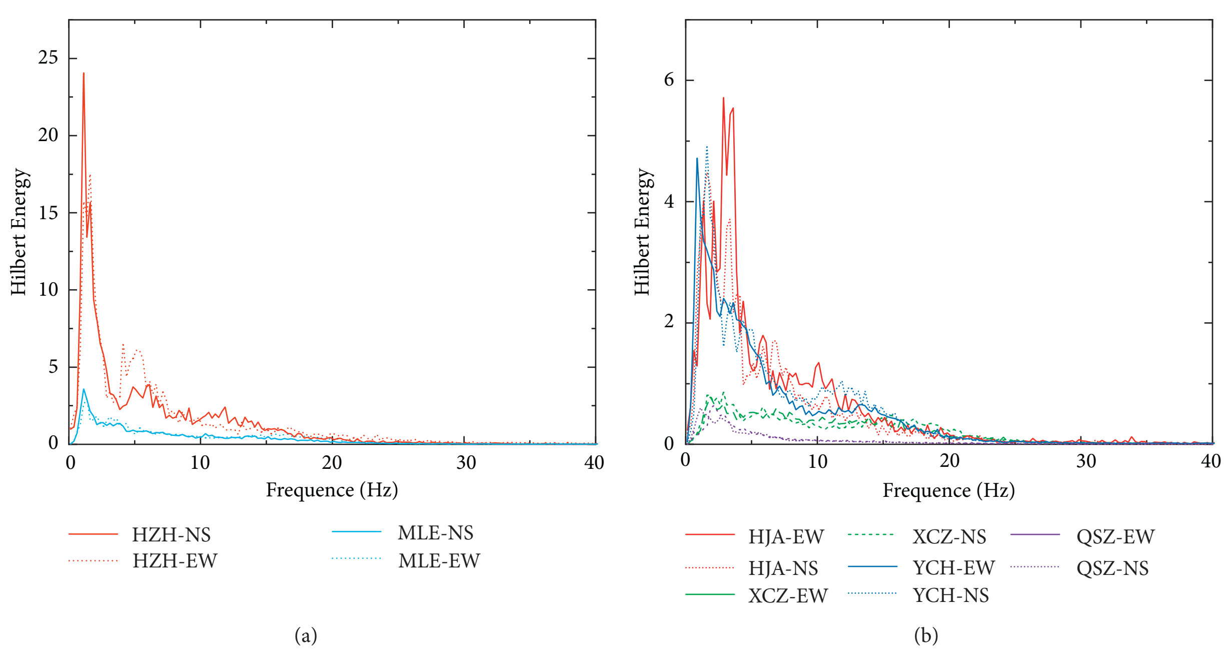

Figure 6: Marginal spectrum of each strong motion station. (a) Ms 5.0 (b) Ms 4.9.

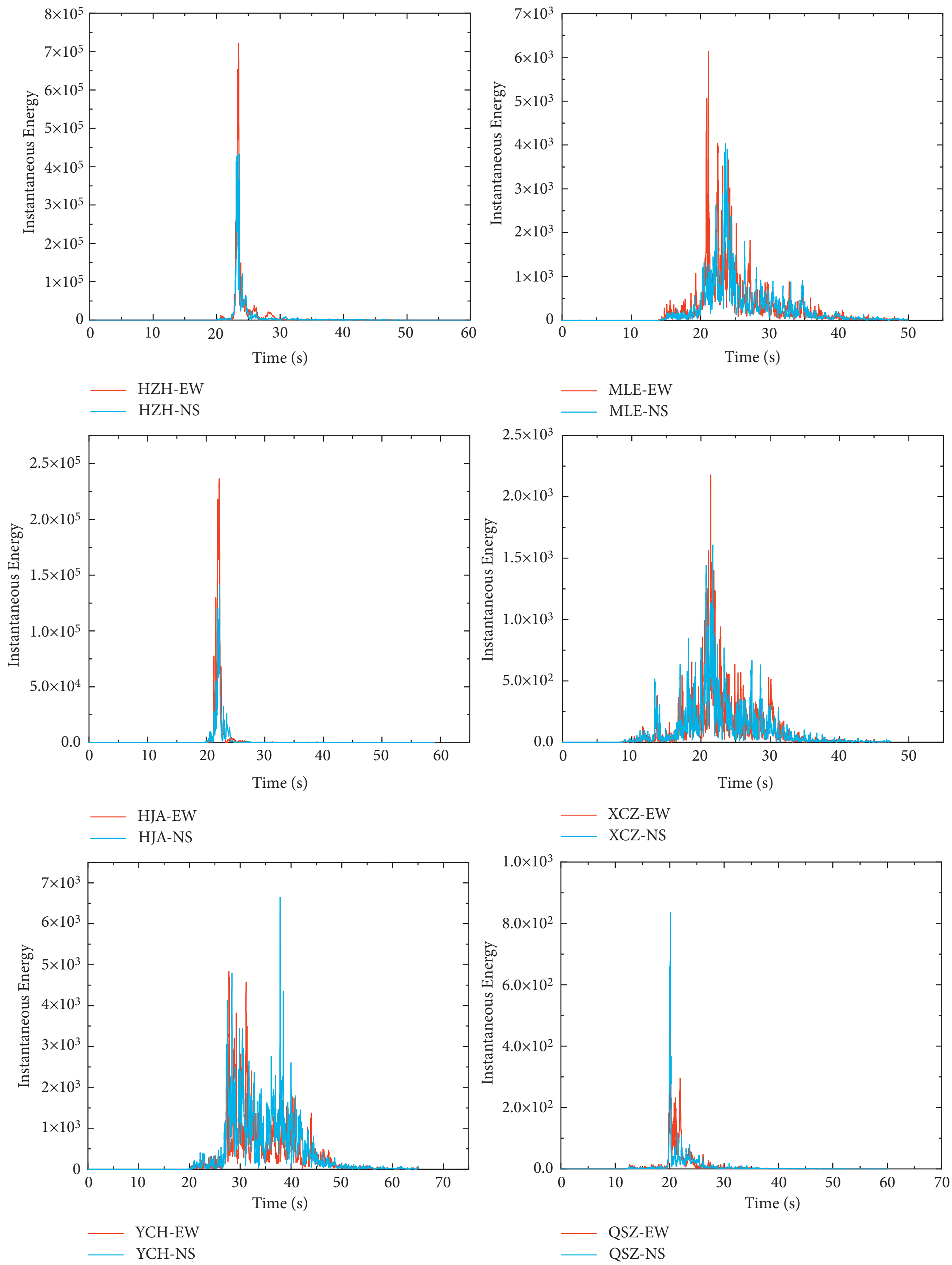

Figure 7: Instantaneous energy spectrum of each strong motion station.

instantaneous energy at QSZ is smaller than XCZ or YCH. This result shows that soil layer can amplify the instantaneous energy.

4.2. Site Characteristics. The HVSR method was often used to investigate the site effect [32]. Similarly, we used horizontal to vertical marginal spectrum ratio based on coda wave to study the site characteristics, because the marginal spectrum can reflect the frequency components more clearly than the Fourier spectrum. The calculation is shown in:

$$R(f) = \frac{H(f)}{V(f)}, \tag{6}$$

where $H(f)$ is the marginal spectrum of horizontal ground motion, $V(f)$ is the marginal spectrum of vertical ground motion.

The time history of seismic wave includes source, propagation path, and site information. Coda wave is a superposition of discontinuous scattered waves formed by the scattering of seismic waves on a nonuniform body in the Earth medium [33]. The generation of coda is related to the incompleteness elasticity, inhomogeneity, and anisotropy of the Earth medium, so coda contains a lot of information about the source and medium. So, coda wave analysis is better than the whole time history of ground motion to obtain the characteristics of the medium. Rautian [34] pointed out that $t >> ts$ (ts is the arrival time of S wave from the time of earthquake occurrence) is the starting point of the coda wave. The starting point and length of coda wave do not have a unified selection method. We select the last 20 s of ground motion as the coda wave in this study, as shown in Figure 8.

The HVSR results based on coda wave using marginal spectrum and the contour map of HVSR in study area are shown in Figures 9 and 10 respectively. It reflects that the predominant frequency of site at each station is within 3.6–6.2 Hz. Although the data are limited, the site characteristics are obvious. The amplification factor (H/V) at rock site (QSZ) is 2, which is minimum among all stations. The factor reaches maximum at HZH which is soil site. The factors at other sites are within 3–5.2. Because of the lack of soil layer thickness data, relationship between the factor and soil layer thickness cannot be discussed further. However, it clearly reflects that soil layer can amplify the ground motion when compared with a rock site. So, HVSR based on coda wave of light-moderate earthquakes using marginal spectrum can be used to investigate the site effect.

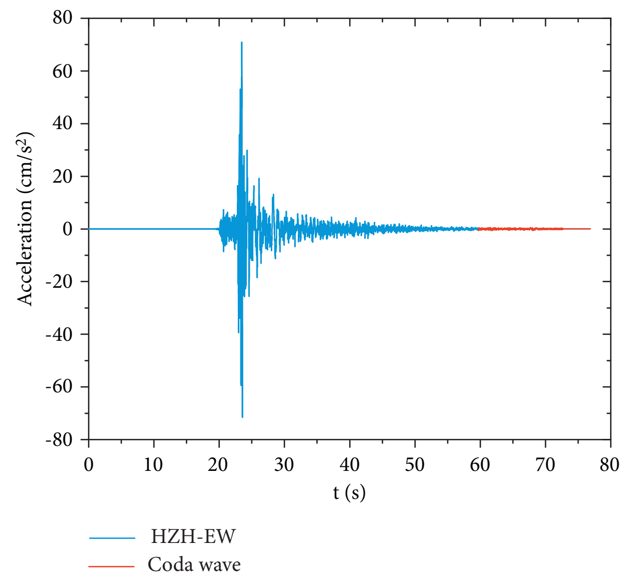

Figure 8: Coda wave.

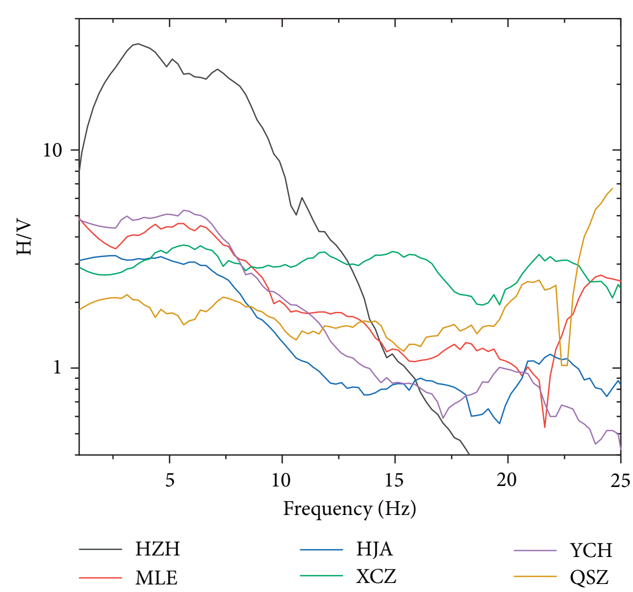

Figure 9: HVSR result based on coda wave using marginal spectrum.

5. Discussion

5.1. Comparison of Predominant Frequency of Ground Motion and Site. The severity of disasters caused by earthquakes is not only related to earthquake intensity but also closely related to ground motion and site characteristics. Site characteristics are related to landform, soil type, soil thickness, stratum structure, and so on. The predominant frequency of site is the comprehensive reflection of these factors. When the predominant frequency of site is close to the seismic ground motion, the resonance effect would be produced and the disaster would also be more serious. Figure 11 presents the HVSR results of HZH and HJA stations and the marginal spectrum of two light-moderate earthquakes in the study. It reflects that the predominant frequencies of the earthquakes are in the low frequency range, which are lower than the predominant frequencies of sites. So, the disasters induced by the two earthquakes are minor.

5.2. Comparison of Fourier Spectrum and Marginal Spectrum. The frequency characteristics of two light-moderate earthquakes in this study are clearly according to the Hilbert-Huang spectrum and marginal spectrum based on HHT.

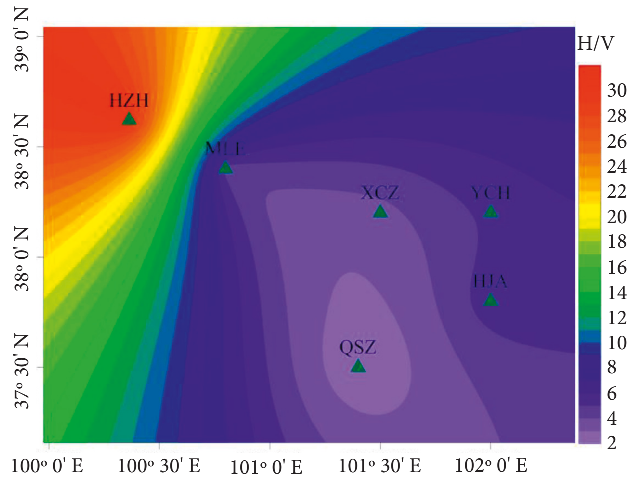

Figure 10: Contour map of HVSR in study area.

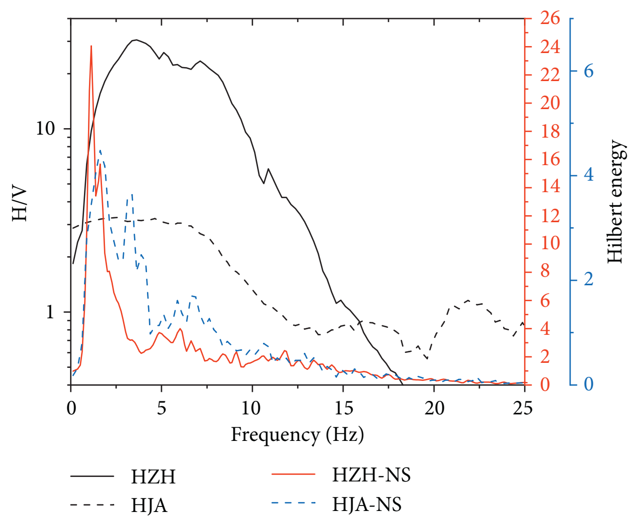

Figure 11: Marginal spectrum and HVSR results.

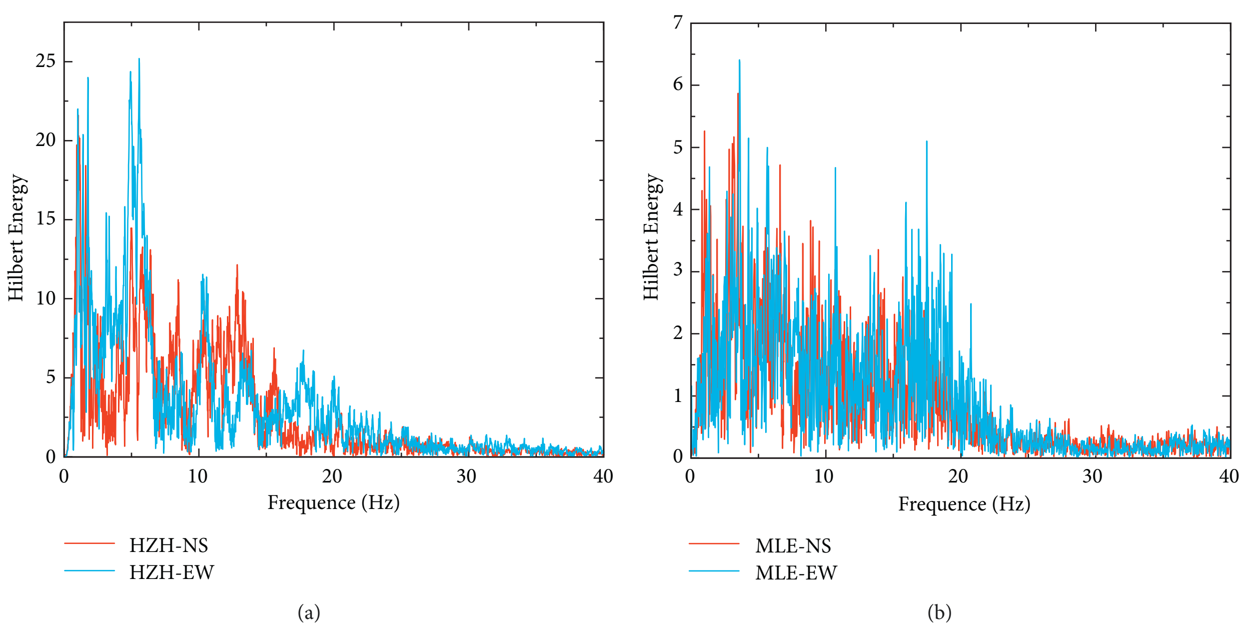

Figure 12: Fourier spectrum of Ms 5.0 earthquake. (a) HZH (b) MLE.

Generally, we use FFT to clarify the frequency characteristics. However, FFT applicable to linear and stationary signal analysis, which cannot present the frequency features of seismic waves for the earthquake signal is nonlinear and nonstationary. In order to clear that, we performed FFT on the seismic waves of Ms 5.0, as it is shown in Figure 12. The prominent frequency of HZH is within 0–8 Hz and the prominent frequency of MLE is within 0–20 Hz. Compared with marginal spectrum that is shown in Figure 6 Fourier spectrum cannot reflect the predominant frequency clearly and the low frequency energy is not well presented. So, HHT is better than FFT in the frequency analysis of seismic waves, which gives a direction for future relative studies.

6. Conclusions

In the study, we analyzed the spectrum characteristics of two light-moderate earthquakes that occurred in loess area of China from time-frequency domain based on HHT and the site characteristics based on the coda wave of the earthquakes using HVSR method. The main conclusions are shown as follows:

(1) Hilbert-Huang spectrum based on HHT can clearly reflect the relationship among time, frequency, and amplitude (instantaneous frequency energy) of seismic waves of light-moderate earthquakes. The energy of seismic wave at strong motion station that close to epicenter is mainly concentrated within 20 Hz. With the increase of epicenter distance, the energy will change from concentration to divergence in time and frequency and gradually decrease at same site condition. In the process of propagation, the energy of a seismic wave is more concentrated under the rock site condition than it under the soil site situation and a loess layer can amplify the energy.

(2) The marginal spectrum distinctly shows the accumulation of energy of light-moderate earthquake in time. Two earthquakes present low prominent frequency characteristics. Peak amplitude of Ms 5.0 earthquake in two directions occurred within 1.125–1.625 Hz, and the value of Ms 4.9 earthquake is within 1.075–2.45 Hz, respectively. With the increase of epicenter distance, Hilbert energy shows a downward trend. The Hilbert energy at soil site is about 3 times greater than at rock site when the epicenter distance is close, which suggests that soil layer can greatly amplify the Hilbert energy of an earthquake.

(3) Instantaneous energy spectrum shows the change law of instantaneous energy of light-moderate earthquakes with time. Instantaneous energy attenuates quickly with the increase of epicenter distance. Site conditions greatly impact on the characteristics of instantaneous energy. Instantaneous energy at the rock site is much smaller than at soil site, which reflects that soil layer can significantly amplify the instantaneous energy of an earthquake.

(4) HVSR based on coda wave of light-moderate earthquakes using marginal spectrum can be used to investigate the site characteristics. The predominant frequency of site at each station is within 3.6–6.2 Hz. Compared with a rock site, soil layer can amplify the ground motion. The amplification factor at rock site is minimum with value 2 and the factor reaches 30.2 at HZH which is soil site.

Data Availability

Basic data can be obtained from the corresponding author upon request.

Conflicts of Interest

The authors declare that they have no conflicts of interest.

Acknowledgments

Data for this study are provided by the Institute of Engineering Mechanics, China Earthquake Administration. This research work was financially supported by the Key Project of National Natural Science Foundation of China (No. U1939209).

References

[1] S. L. Kramer and M. W. Smith, "Modified Newmark model for seismic displacements of compliant slopes," *Journal of Geotechnical and Geoenvironmental Engineering*, vol. 123, no. 7, pp. 635–644, 1997.

[2] R. D. Borcherdt, "Estimates of site dependent response spectra for design (methodology and justification)," *Earthquake Spectra*, vol. 10, no. 4, pp. 617–653, 1994.

[3] T. I. Allen and D. J. Wald, "On the use of high-resolution topographic data as a proxy for seismic site conditions (VS30)," *Bulletin of the Seismological Society of America*, vol. 99, no. 2A, pp. 935–943, 2009.

[4] Y. Gao, Z. L. Wu, Z. Liu, and H. Zhou, "Seismic source characteristics of nine strong earthquakes from 1988 to 1990 and earthquake activity since 1970 in the sichuan-qinghai-xizang (tibet) zone of China," *Pure and Applied Geophysics*, vol. 157, no. 9, pp. 1423–1443, 2000.

[5] V. M. Smirnov, E. V. Smirnova, M. N. Tsidilina, and M. V. Gaponova, "Seismo-ionospheric variations during strong earthquakes based on the example of the 2010 earthquake in Chile," *Cosmic Research*, vol. 56, no. 4, pp. 267–275, 2018.

[6] S. T. Akopian, "Detection of features of the strong earthquake of march 25, 2020, east of the kuril islands using the seismic entropy method," *Seismic Instruments*, vol. 56, no. 5, pp. 620–631, 2020.

[7] Lanzhou Institute of Seismology, *Catalogue of strong Earthquakes in Shaanxi, Gansu, Ningxia and Qinghai Provinces (1177 BC-1982),* Shaanxi Science and Technology Press, Xian, China, 1985.

[8] X. Y. Du and S. L. Huang, "Risk factors of earthquake and the management of its secondary disasters," *Journal of Catastrophology*, vol. 23, pp. 71–74, 2008.

[9] A. Beckers, C. Beck, A. F. Hubert et al., "Sedimentary impacts of recent moderate earthquakes from the shelves to the basin

floor in the western Gulf of Corinth," *Marine Geology*, vol. 384, pp. 81–102, 2017.

[10] Q. Guo, L. F. Chernogor, K.-P. Garmash, V. Rozumenko, and Y. Zheng, "Dynamical processes in the ionosphere following the moderate earthquake in Japan on 7 July 2018," *Journal of Atmospheric and Solar-Terrestrial Physics*, vol. 186, pp. 88–103, 2019.

[11] D. Bindi, F. Cotton, S. R. Kotha, C. Bosse, D. Stromeyer, and G. Grunthal, "Application-driven ground motion prediction equation for seismic hazard assessments in non-cratonic moderate-seismicity areas," *Journal of Seismology*, vol. 21, no. 5, pp. 1201–1218, 2017.

[12] V. Shukla, V. Chauhan, N. Kumar, and D. Hazarika, "Assessment of Rn-222 continuous time series for the identification of anomalous changes during moderate earthquakes of the Garhwal Himalaya," *Applied Radiation and Isotopes*, vol. 166, Article ID 109327, 2020.

[13] R. K. L. Su, T. O. Tang, and K. C. Liu, "Simplified seismic assessment of buildings using non-uniform Timoshenko beam model in low-to-moderate seismicity regions," *Engineering Structures*, vol. 120, pp. 116–132, 2016.

[14] Q. J. Chen, W. Z. Yuan, Y. C. Li, and Ly Cao, "Dynamic response characteristics of super high-rise buildings subjected to long-period ground motions," *Journal of Central South University*, vol. 20, no. 5, pp. 1341–1353, 2013.

[15] M. G. Tian and W. J. Yi, "Dynamic behavior of reinforced concrete frame structure during construction," *Journal of Central South University of Technology*, vol. 15, no. 3, pp. 418–422, 2008.

[16] N. E. Huang, Z. Shen, S. R. Long et al., "The empirical mode decomposition and the Hilbert spectrum for nonlinear and non-stationary time series analysis," *Proceedings of the Royal Society of London. Series A: Mathematical, Physical and Engineering Sciences*, vol. 454, no. 1971, pp. 903–995, 1998.

[17] J. C. Chen, L. M. Wang, P. Wang, and A. L. Che, "Failure mechanism investigation on loess–mudstone landslides based on the Hilbert–Huang transform method using a large-scale shaking table test," *Engineering Geology*, vol. 302, Article ID 106630, 2022.

[18] S. R. Garcia, M. P. Romo, and L. Alcántara, "Analysis of non-linear and non-stationary seismic recordings of Mexico City," *Soil Dynamics and Earthquake Engineering*, vol. 127, Article ID 105859, 2019.

[19] D. Q. Song, X. L. Liu, J. Huang, and J. M. Zhang, "Energy-based analysis of seismic failure mechanism of a rock slope with discontinuities using Hilbert-Huang transform and marginal spectrum in the time-frequency domain," *Landslides*, vol. 18, no. 1, pp. 105–123, 2021.

[20] G. Fan, J. J. Zhang, J. B. Wu, and K. M. Yan, "Dynamic response and dynamic failure mode of a weak intercalated rock slope using a shaking table," *Rock Mechanics and Rock Engineering*, vol. 49, no. 8, pp. 3243–3256, 2016.

[21] X. L. Li, S. J. Chen, S. Liu, and Z. H. Li, "AE waveform characteristics of rock mass under uniaxial loading based on Hilbert-Huang transform," *Journal of Central South University*, vol. 28, no. 6, pp. 1843–1856, 2021.

[22] S. M. Liu, X. L. Li, and D. K. Wang, "Investigations on the mechanism of the microstructural evolution of different coal ranks under liquid nitrogen cold soaking," *Energy Sources, Part A: Recovery, Utilization, and Environmental Effects*, pp. 1–17, 2020.

[23] X. L. Li, S. J. Chen, Q. M. Zhang, X. Gao, and F. Feng, "Research on theory, simulation and measurement of stress behavior under regenerated roof condition," *Geomechanics and Engineering*, vol. 26, no. 1, pp. 49–61, 2021.

[24] X. L. Li, S. J. Chen, S. Wang, M. Zhao, and H. Liu, "Study on in situ stress distribution law of the deep mine taking Linyi Mining area as an example," *Advances in Materials Science and Engineering*, vol. 2021, no. 4, pp. 1–11, Article ID 5594181, 2021.

[25] H. Y. Liu, B. Y. Zhang, X. L. Li et al., "Research on roof damage mechanism and control technology of gob-side entry retaining under close distance gob," *Engineering Failure Analysis*, vol. 138, no. 5, Article ID 106331, 2022.

[26] Y. Nakmura, "A method for dynamic characteristics estimation of subsurface using microtremor on the ground surface," *Quarterly Report of RTRI*, vol. 30, no. 1, pp. 25–33, 1989.

[27] L. F. Bonilla, J. H. Steidl, G. T. Lindley, A. G. Tumarkin, and R. J. Archuleta, "Site amplification in the San Fernando Valley, California: variability of Site-effect estimation using the s-wave, coda, and H/V methods," *Bulletin of the Seismological Society of America*, vol. 87, no. 3, pp. 710–730, 1997.

[28] J. Lermo and F. J. C. García, "Site effect evaluation using spectral ratios with only one station," *Bulletin of the Seismological Society of America*, vol. 83, no. 5, pp. 1574–1594, 1993.

[29] X. J. Li, "Thoughts on the research of earthquake damage phenomenon and engineering earthquake in recent years," *International earthquake dynamics*, vol. 8, pp. 26–31, 2001.

[30] A. Ayenu and N. A. Attoh, "Criterion for selecting relevant intrinsic mode functions in empirical mode decomposition," *Advances in Adaptive Data Analysis*, vol. 02, no. 01, pp. 1–24, 2010.

[31] H.-X. Liu, Q. Xu, X. Zhu, X. P. Zhou, and W. D. Liu, "Marginal spectrum characteristics of the rock slope with a soft interlayer during an earthquake," *Rock and Soil Mechanics*, vol. 40, no. 4, pp. 1387–1396, 2019.

[32] L. Agostini, J. Boaga, A. Galgaro, and A. Ninfo, "HVSR technique in near-surface thermal-basin characterization: the example of the Caldiero district (North-East Italy)," *Environmental Earth Sciences*, vol. 74, no. 2, pp. 1199–1210, 2015.

[33] K. Aki, "Analysis of the seismic coda of local earthquakes as scattered waves," *Journal of Geophysical Research*, vol. 74, no. 2, pp. 615–631, 1969.

[34] T. G. Rautian and V. I. Khalturin, "The use of the coda for determination of the earthquake source spectrum," *Bulletin of the Seismological Society of America*, vol. 68, no. 4, pp. 923–948, 1978.